Flow Reversals in Turbulent Convection via Vortex Reconnections

Mani Chandra* and Mahendra K. Verma†

Department of Physics, Indian Institute of Technology, Kanpur 208016, India

(Received 17 July 2012; published 14 March 2013)

We employ detailed numerical simulations to probe the mechanism of flow reversals in two-dimensional turbulent convection. We show that the reversals occur via a vortex reconnection of two attracting corner rolls having the same sign of vorticity, thus leading to major restructuring of the flow. Large fluctuations in heat transport are observed during the reversal due to the flow reconfiguration. The flow configurations during the reversals have been analyzed quantitatively using large-scale modes. Using these tools, we also show why flow reversals occur for a restricted range of Rayleigh and Prandtl numbers.

DOI: 10.1103/PhysRevLett.110.114503 PACS numbers: 47.55.P−, 47.27.De

Several experiments [1–8] and numerical simulations [8–12] on turbulent convection exhibit ''flow reversals'' in which the probes near the lateral walls of the container show random reversals (also see review articles [13]). These reversals have certain similarities with magnetic field reversals in dynamo and Kolmogorov flow [7]. Researchers typically study convection in a controlled setup called Rayleigh-Bénard convection in which a fluid confined between two plates is heated from below and cooled at the top. The two nondimensional numbers used to characterize the flow are the Rayleigh number (Ra), which is the ratio of the buoyancy term and the diffusive term, and the Prandtl number (Pr), which is the ratio of the kinematic viscosity and the thermal diffusivity. Flow reversals have been observed in many convection experiments in a cylindrical geometry for $\mathrm{Ra} > 10^8$ [1–4]. However, in box geometry, flow reversals occur for a limited range of Prandtl number, Rayleigh number, and aspect ratio [5,7,8].

Several theoretical models have been invoked to explain flow reversals [9,14,15]. Reversals have been classified into two categories: rotation-led reversals which occur in a cylinder, and cessation-led reversals which occur in both a cylinder and a box [3,8,11,12]. In cessation-led reversals, the primary mode of the flow disappears with an emergence of secondary modes during the reversals. This is similar to the emergence of quadrupolar mode during dynamo reversals [7].

One important question that persists is, why do flow reversals occur in a restricted parameter regime? In this Letter, we explain this through a quantitative investigation of the convective flow structures for a range of parameters using Fourier decomposition. This scheme allows for accurate representation of the flow [12] and enables us to quantify parameter regimes of reversals in terms of Fourier mode amplitudes. In addition, we show that flow reversals occur via vortex reconnections, and we connect them to vortex dynamics. We also observe large fluctuations in heat transport during a reversal as a result of the flow reorganization during the event. We restrict our study to 2D flow reversals whose flow structures are well represented by experiments conducted in quasi-two-dimensional geometry [8].

We solve the equations governing Rayleigh-Bénard convection under Boussinesq approximation [12] in a 2D box of aspect ratio 1 with no-slip walls on all sides. The side walls are insulating, while the top and the bottom conducting walls are maintained at constant temperatures. The simulations are performed using NEK5000 [16] that employs the spectral element method. We use a 28×28 spectral element with a seventh order polynomial; thus, we have an effective grid of 196×196 points. The grid density is higher at the boundaries in order to resolve the boundary layers. We perform simulations for $\mathrm{Pr} = 1$ and Ra ranging from 10^4 to 10^9.

To quantify the flow structures, we project the nondimensionalized horizontal velocity (u), vertical velocity (v), and temperature (T) onto the following basis:

$$u = \sum_{m,n} \hat{u}_{m,n} \sin(m\pi x) \cos(n\pi y), \tag{1}$$

$$(v, T) = \sum_{m,n} (\hat{v}_{m,n}, \hat{T}_{m,n}) \cos(m\pi x) \sin(n\pi y). \tag{2}$$

It has been shown that the above basis is a good representative of the flow field in a box geometry [12]. The mode with wave number (m, n) corresponds to a flow structure with m rolls in the x direction and n rolls in the y direction. In the following discussion we will use the above basis to analyze the mechanism of flow reversals as well as the range of Pr and Ra for which reversals take place.

To understand the limited range of Ra and Pr for the occurrence of reversals, we invoke the critical role played by the ''corner rolls'' [represented by $(m = 2, n = 2)$ mode] in the reversal dynamics [8,12]. In particular, the relative strength of the (2,2) mode with respect to the dominant mode determines if a reversal will occur or not. We observe three distinct flow structures for the range of $\mathrm{Ra} = (10^4$–$10^9)$ performed in our simulations. The mode (1,1), representing a large single role, is dominant until $\mathrm{Ra} \sim 10^5$ [Fig. 1(a)]. After this, the mode (1,2),

 © 2013 American Physical Society

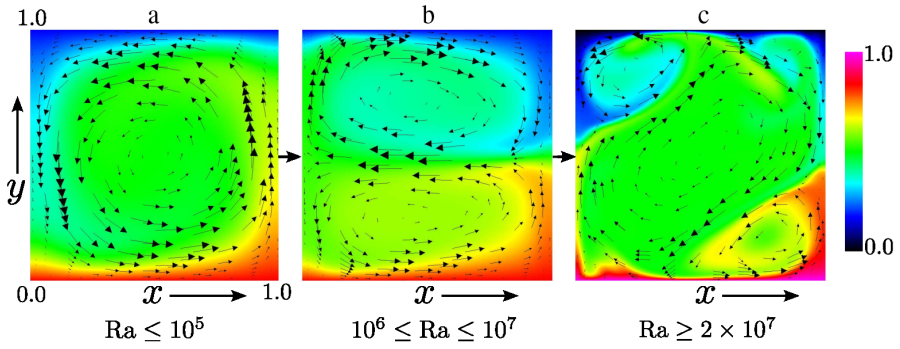

FIG. 1 (color online). Steady state flow structures at different Rayleigh numbers: (a) for $\mathrm{Ra} \leq 10^5$, a single roll with the dominant ($m = 1$, $n = 1$) mode, (b) for $10^6 \leq \mathrm{Ra} \leq 10^7$, two rolls stacked on top of each other corresponding to the mode (1,2), and (c) for $\mathrm{Ra} \geq 2 \times 10^7$, two corner rolls with a dominant roll aligned along the 45 deg diagonal, a configuration dominated by the modes (1,1) and (2,2).

representing two horizontally stacked rolls, dominates until $\mathrm{Ra} \approx 10^7$ [Fig. 1(b)]. The mode (2,2), which is a dominant player for the flow reversals, is born only after $\mathrm{Ra} \approx 2 \times 10^7$ [Fig. 1(c)], which is the reason for the absence of reversals for lower Ra. The transition to the reversal state is seen clearly in the bifurcation diagram (Fig. 2). The bifurcation that leads to the birth of the (2,2) mode and hence reversals is indicated by the vertical dotted line in the plot. The phase space projections of the structures at various Rayleigh numbers are quite different. The system exhibits fixed point and quasiperiodic behavior for $\mathrm{Ra} = 10^4$ and 10^7, respectively, but it becomes chaotic for $\mathrm{Ra} = 2 \times 10^7$, with the system jumping between the two flow reversing states [17]. The sequence of bifurcations described here is quite similar to those presented by Paul *et al.* [18] for 2D convection.

In the third regime, $\mathrm{Ra} \geq 2 \times 10^7$, the mode $\hat{v}_{1,1}$ grows faster than that of the mode $\hat{v}_{2,2}$ with an increase in the Rayleigh number (see Fig. 2). Quantitatively, the averaged value of $|\hat{v}_{2,2}|/|\hat{v}_{1,1}|$ falls monotonically from 0.45 at $\mathrm{Ra} = 2 \times 10^7$ to 0.10 at $\mathrm{Ra} = 10^9$ [17]. The increase of $\hat{v}_{1,1}$ relative to $\hat{v}_{2,2}$ may be due to an inverse cascade of energy. This result indicates that for higher Ra, the corner rolls become weaker compared to the (1,1) mode. Therefore, reversals are observed only for a narrow band near $\mathrm{Ra} = 2 \times 10^7$ where the (2,2) mode is sufficiently strong. We observe similar behavior for $\mathrm{Pr} = 10$ except that the (2,2) mode appears for $\mathrm{Ra} \approx 10^6$, a value lower than that for $\mathrm{Pr} = 1$. Consequently, the range of Ra exhibiting flow reversals is broader for $\mathrm{Pr} = 10$ compared to $\mathrm{Pr} = 1$, consistent with the results of Sugiyama *et al.* [8].

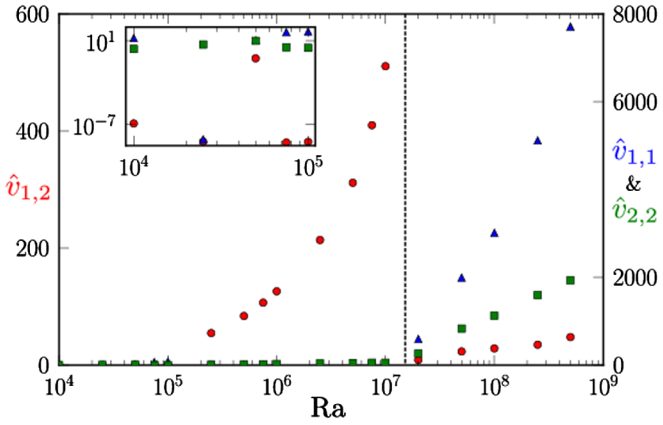

FIG. 2 (color online). A bifurcation diagram for the modes $\langle|\hat{v}(1,1)|\rangle$ (blue triangles), $\langle|\hat{v}(2,2)|\rangle$ (green squares), and $\langle|\hat{v}(1,2)|\rangle$ (red circles) as a function of the Rayleigh number Ra for $\mathrm{Pr} = 1$. Here $\langle\cdot\rangle$ is the temporal average. We observe that $0 \leq \langle|\hat{v}(1,2)|\rangle \leq 600$ (left axis), while $0 \leq \langle|\hat{v}(1,1)|\rangle \leq 8000$ and $0 \leq \langle|\hat{v}(2,2)|\rangle \leq 2000$ (both right axis). The system bifurcates to reversal states around the vertical dashed line.

Now we probe in detail the process of flow reversal by studying the flow structures of six snapshots during one of the reversals (see Fig. 3). A movie of the flow reversal can be downloaded from Ref. [19]. The starting point of the reversal is the stable configuration shown in Fig. 1(c), corresponding to $t = 0$ of Fig. 4. At first, the mode (2,2) (or the corner rolls) grows at the expense of the mode (1,1), as evident from Figs. 3(a) and 3(b). The top-left and bottom-right corner rolls have vorticity in the same direction; hence, they attract each other and come close due to vortex dynamics in 2D [20]. Since the velocities of the streamlines are directed in opposite directions, they reconnect, thus converting two corner rolls into a single roll [see Fig. 3(c)]. As a result of the reconnection, the new large roll has the cumulative vorticity in the same direction as the reconnecting rolls. The reconnection event leads to a change in the flow topology, and is similar to 2D magnetic field reconnections in magnetohydrodynamics [21]. The new large roll aligned along the -45 deg diagonal [Fig. 3(c)] has vorticity opposite that of the large roll before the reversal [Fig. 1(c)]. The process of reversal, from the state corresponding to Fig. 1(c) to the state 3(f), takes approximately 0.01 thermal diffusive time units (see Fig. 4). This interval is only a fraction of time interval between consecutive reversals, which averages to approximately 0.6 thermal diffusive time units [12]. The

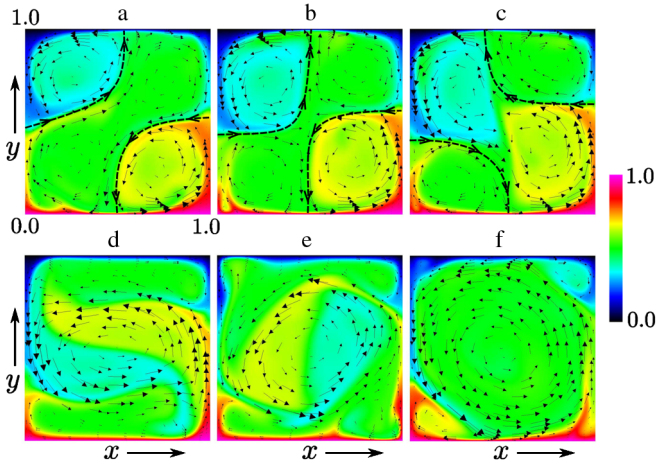

FIG. 3 (color online). Six snapshots of the velocity and temperature profiles during the reversal at $t = 0.003\,41$ (a), 0.003 82 (b), 0.004 02 (c), 0.004 44 (d), 0.004 77 (e), 0.01 (f) in thermal diffusive time units. The reversal process starts at $t = 0$ with the flow profile shown in Fig. 1(c): (a), (b) Growth of corner rolls; (c) the two corner rolls at the upper-left and bottom-right corners reconnect to form a large single roll. The streamlines, represented by black curves, combine via vortex reconnections. (d), (e) The flow reconfigures itself via rotation of the large roll formed after the reconnection. There is a strong nonlinear interaction among the modes (1,1), (2,2), (1,3), and (3,1) during these events. (f) The flow stabilizes to a configuration with the dominant roll aligned along -45 deg diagonal.

probability distribution of the time intervals between two consecutive reversals is expected to be a Poissonian, as seen in cessation-led reversals [3].

The strength of the new roll grows along with an emergence of two new secondary modes (1,3) and (3,1), which are generated as a result of triad interaction with the condition $\mathbf{k} = \mathbf{p} + \mathbf{q}$ [12]. Note that $(1,3) = (2,2) + (-1,1)$ and $(3,1) = (2,2) + (1,-1)$. The subsequent rotation of the newly formed roll leads to the flow configurations of Figs. 3(d) and 3(e), which are dominated by (1,1), (2,2), (1,3), and (3,1) modes [17]. After around 0.01 thermal diffusive time units, the system transforms to a roll aligned along -45 deg diagonal with an opposite vorticity [Fig. 3(f)] compared to the original one [Fig. 1(c)]. The process would repeat for the next reversal with a difference that the bottom-left and the top-right corner rolls would reconnect during the next reversal.

The modes (1,1) and (2,2) are the most dominant ones, except during reversals, with the (1,1) mode switching sign between reversals [17]. The sign of the (2,2) mode or the sense of rotation of the corner rolls, however, remains unchanged after the reversal, as shown through symmetry arguments [12]. Another surprising observation is that the amplitude of the (2,2) mode is always positive. As a result, the hot plume of the corner rolls (at the bottom plate) always ascends via the vertical walls, and the cold plume descends via the vertical walls [see Figs. 1(c) and 3(f)]. This seems to be a generic feature of many convection simulations and experiments, but its mathematical justification eludes us at the present.

We now discuss heat transport during a reversal. The global Nusselt number Nu exhibits large fluctuations including negative values during a short time interval [see Fig. 4(a)]. Here, $\mathrm{Nu} = \int[(-d\bar{T}(y)/dy) + vT]d\mathbf{r}$, where nondimensionalized $\bar{T}(y)$ is the averaged temperature over the cross section at height y. The negative Nusselt number occurs for the flow configurations resembling Fig. 3(e) in which the hot fluid parcel in the middle of the box descends while the cold parcel ascends, contrary to generic situations when the hot parcels ascend and the cold ones descend. Negative Nu may appear contradictory, but it could be understood in terms of the heat flux through the cross section at height y, $\mathrm{Nu}(y) = -d\bar{T}(y)/dy + \int_x v(x,y)T(x,y)dx$; here, $\int_x$ is the integral over the line at height y. We compute this quantity for various horizontal cross sections for the flow configurations corresponding to Figs. 3(a)–3(f). As illustrated in Fig. 4(b), Nu(y) fluctuates significantly in the bulk for flow configurations (c, d, e) during the reversals, with strong positive values for (d), to

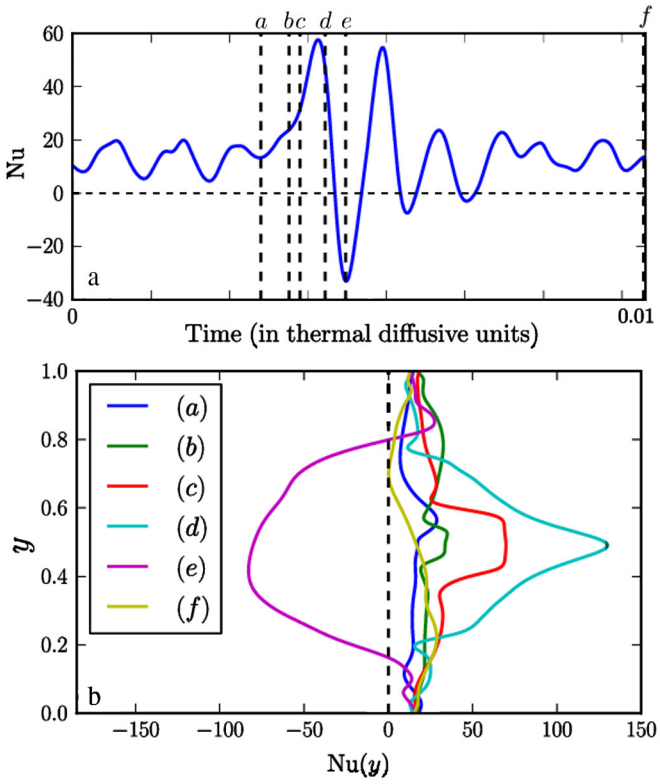

FIG. 4 (color online). (a) Time series of the global Nusselt number. (b) Plot of Nu(y) (the normalized heat transport for the cross section at height y) versus y during the reversal. The six curves represent the six snapshots of Fig. 3. The flow reconfigurations during the reversal lead to large fluctuations in Nu(y) in the bulk, ranging from strong positive values for (d) to strong negative values for (e). Note, however, that the Nu(y) is positive near both the plates ($y \to 0, 1$).

strong negative values for (e). Note, however, that Nu(y) is positive near the top and bottom plates for all cases. The large fluctuations in Nu(y) in the bulk are a result of the rotation of the central role formed after reconnection. We remark that the negative Nu for the two-dimensional convective flow is due to strong geometrical constraints faced by the rolls during the reversals, and may not be present in a convection experiment in a cylindrical geometry.

In summary, we show that flow reversals are caused by vortex reconnections of two attracting rolls. The flow reconfigurations during the reversals are due to the nonlinear interactions among the large-scale modes (1,1), (2,2), (1,3), and (3,1). We find large fluctuations in heat transport during the reversals, which are due to the above restructuring of the flow. The (2,2) mode, critical for the dynamics of flow reversals, is born after $\mathrm{Ra} = 2 \times 10^7$ (for $\mathrm{Pr} = 1$), and its strength relative to the (1,1) mode decreases monotonically afterwards. This is the reason that flow reversals are observed only for a limited range of parameter values.

The role of the large-scale modes described in the present Letter is analogous to the ''cessation-led reversal'' observed in turbulent convection in cylinder [11] as well as in dynamo reversals [7], where the quadrupolar mode [equivalent to the (2,2) mode] dominates the dipolar mode [equivalent to the (1,1) mode] during the reversal. Future work for different geometries, and Prandtl and Rayleigh numbers, would provide valuable insights that will help us build a comprehensive theory of reversals in convection and dynamo.

We thank Annick Pouquet, Stephan Fauve, and Jörg Schumacher for useful discussions. We also thank the Centre for Development of Advanced Computing (CDAC) and the Computer Center of IIT Kanpur for providing computing time. Part of this work was supported by a Swarnajayanti fellowship to M. K. V. and BRNS grant BRNS/PHY/20090310.

*Present address: Astronomy Department, University of Illinois, 1002 West Green Street, Urbana, IL 61801, USA.
†mkv@iitk.ac.in

[1] S. Cioni, S. Ciliberto, and J. Sommeria, J. Fluid Mech. **335**, 111 (1997).
[2] J. J. Niemela, L. Skrbek, K. R. Sreenivasan, and R. J. Donnelly, J. Fluid Mech. **449**, 169 (2001).
[3] E. Brown, A. Nikolaenko, and G. Ahlers, Phys. Rev. Lett. **95**, 084503 (2005); E. Brown and G. Ahlers, J. Fluid Mech. **568**, 351 (2006); Phys. Rev. Lett. **98**, 134501 (2007).
[4] H. D. Xi and K. Q. Xia, Phys. Rev. E **75**, 066307 (2007).
[5] A. Vasiliev and P. Frick, J. Phys. Conf. Ser. **318**, 082013 (2011).
[6] T. Yanagisawa, Y. Yamagishi, Y. Hamano, Y. Tasaka, M. Yoshida, K. Yano, and Y. Takeda, Phys. Rev. E **82**, 016320 (2010).
[7] B. Gallet, J. Herault, C. Laroche, F. Pétrélis, and S. Fauve, Geophys. Astrophys. Fluid Dyn. **106**, 468 (2012).
[8] K. Sugiyama, R. Ni, R. J. A. M. Stevens, T. S. Chan, S.-Q. Zhou, H.-D. Xi, C. Sun, S. Grossmann, K.-Q. Xia, and D. Lohse, Phys. Rev. Lett. **105**, 034503 (2010).
[9] R. Benzi and R. Verzicco, Europhys. Lett. **81**, 64 008 (2008).
[10] M. Breuer and U. Hansen, Europhys. Lett. **86**, 24 004 (2009).
[11] P. K. Mishra, A. K. De, M. K. Verma, and V. Eswaran, J. Fluid Mech. **668**, 480 (2011).
[12] M. Chandra and M. K. Verma, Phys. Rev. E **83**, 067303 (2011).
[13] G. Ahlers, S. Grossmann, and D. Lohse, Rev. Mod. Phys. **81**, 503 (2009); D. Lohse and K. Q. Xia, Annu. Rev. Fluid Mech. **42**, 335 (2010).
[14] K. R. Sreenivasan, A. Bershadskii, and J. J. Niemela, Phys. Rev. E **65**, 056306 (2002).
[15] F. F. Araujo, S. Grossmann, and D. Lohse, Phys. Rev. Lett. **95**, 084502 (2005).
[16] P. F. Fischer, J. Comput. Phys. **133**, 84 (1997); http://nek5000.mcs.anl.gov/.
[17] See Supplemental Material at http://link.aps.org/supplemental/10.1103/PhysRevLett.110.114503 for phase space plots (Figs. 1 and 2), plot of $|\hat{v}_{2,2}|/|\hat{v}_{1,1}|$ versus Ra (Fig. 3), and the time series of the mode amplitudes and Nu (Fig. 4).
[18] S. Paul, M. K. Verma, P. Wahi, S. Reddy, and K. Kumar, Int. J. Bifurcation Chaos Appl. Sci. Eng. **22**, 1230018 (2012).
[19] http://turbulence.phy.iitk.ac.in/animations:convection (video-1).
[20] H. Aref and I. Zawadzki, in *New Approaches and Concepts in Turbulence*, edited by T. Dracos and A. Tsinober (Birkhäuse, Basel, 1993).
[21] E. Priest and T. Forbes, *Magnetic Reconnection: MHD Theory and Applications* (Cambridge University Press, Cambridge, England, 2000).